

A size of ~ 1 AU for the radio source Sgr A* at the centre of the Milky Way

Zhi-Qiang Shen¹, K. Y. Lo², M.-C. Liang³, Paul T. P. Ho^{4,5}, J.-H. Zhao⁴

¹ Shanghai Astronomical Observatory, 80 Nandan Road, Shanghai 200030, China

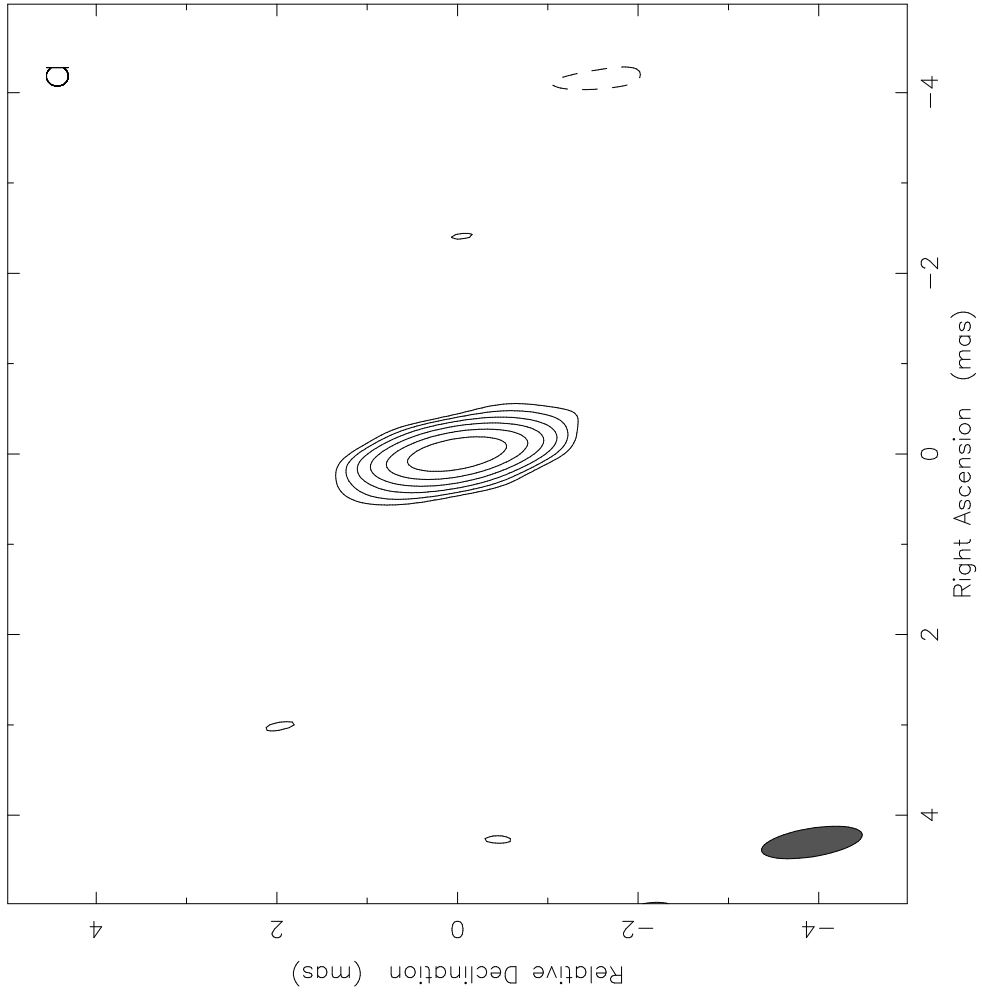
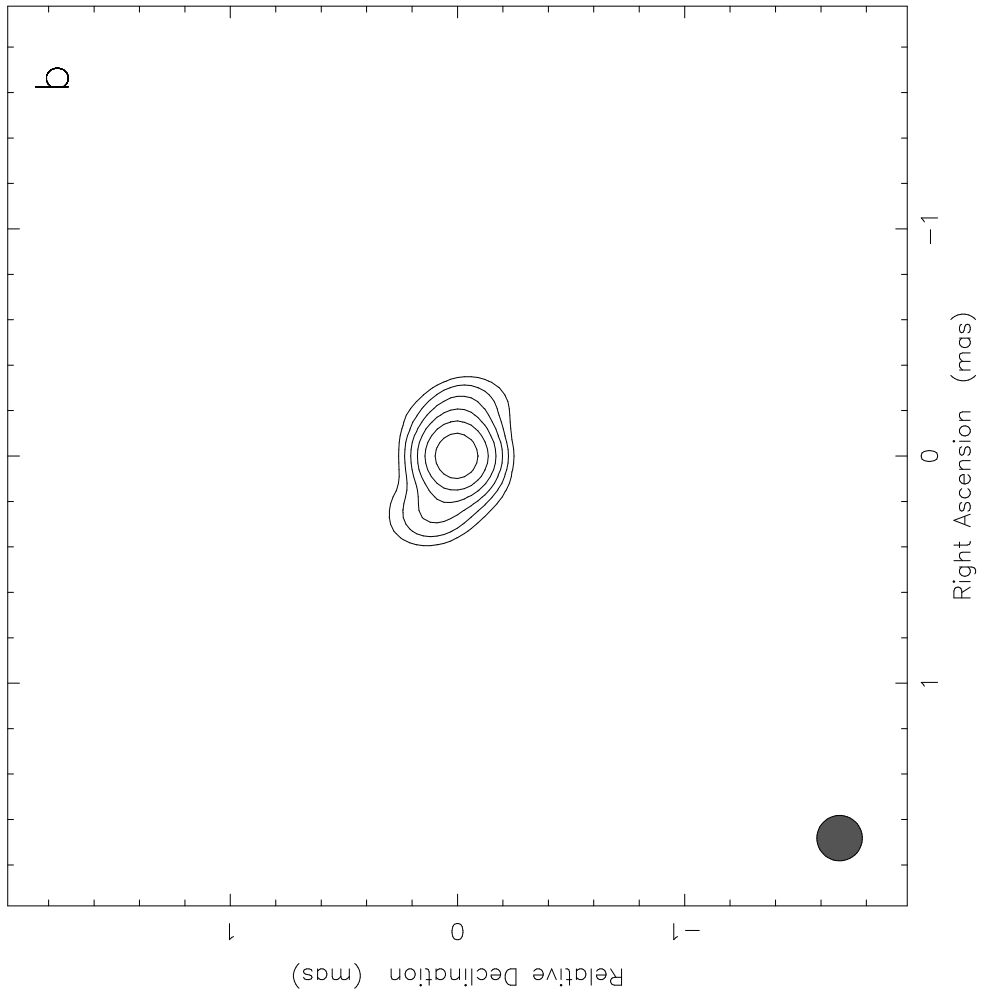
² National Radio Astronomy Observatory, 520 Edgemont Road, Charlottesville, VA 22903, USA

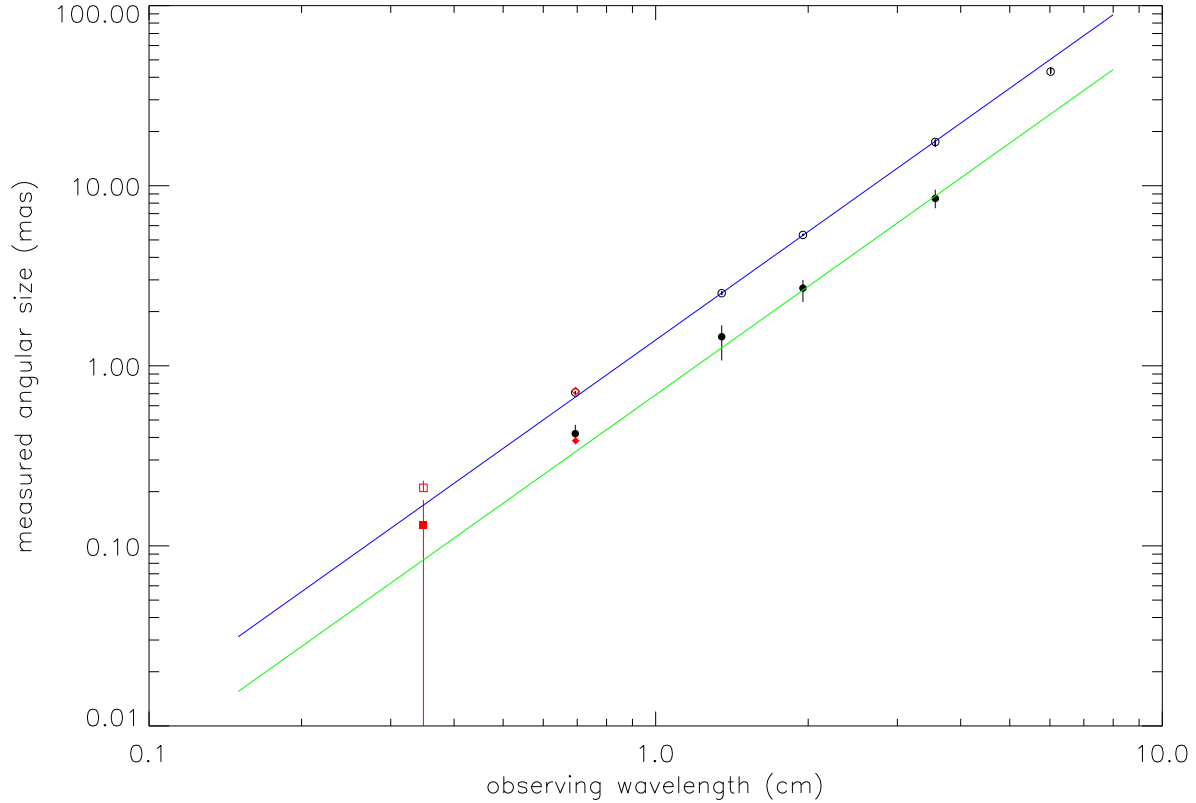
³ Division of Geological and Planetary Sciences, California Institute of Technology, Pasadena, CA 91125, USA

⁴ Harvard-Smithsonian CfA, 60 Garden Street, Cambridge, MA 02138, USA

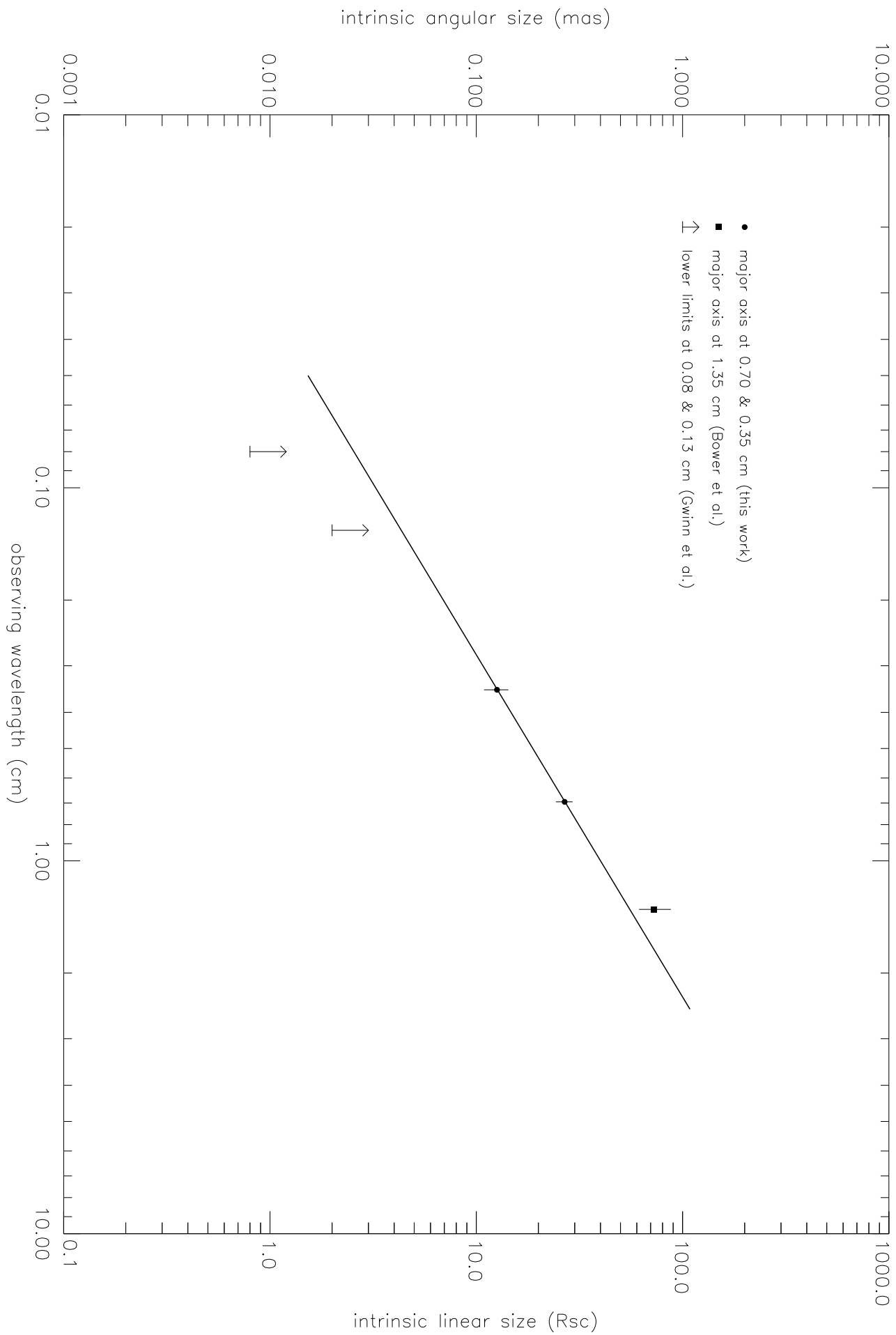
⁵ Institute of Astronomy & Astrophysics, Academia Sinica, PO Box 23-141, Taipei 106, Taiwan, China

Although it is widely accepted that most galaxies have supermassive black holes (SMBHs) at their centers¹⁻³, concrete proof has proved elusive. Sagittarius A* (Sgr A*)⁴, an extremely compact radio source at the center of our Galaxy, is the best candidate for proof⁵⁻⁷, because it is the closest. Previous Very Long Baseline Interferometry (VLBI) observations (at 7mm) have detected that Sgr A* is 2 astronomical unit (AU) in size⁸, but this is still larger than the "shadow" (a remarkably dim inner region encircled by a bright ring) arising from general relativistic effects near the event horizon⁹. Moreover, the measured size is wavelength dependent¹⁰. Here we report a radio image of Sgr A* at a wavelength of 3.5mm, demonstrating that its size is ~ 1 AU. When combined with the lower limit on its mass¹¹, the lower limit on the mass density is 6.5×10^{21} Msun pc⁻³, which provides the most stringent evidence to date that Sgr A* is an SMBH. The power-law relationship between wavelength and intrinsic size (size \propto wavelength^{1.09}), explicitly rules out explanations other than those emission models with stratified structure, which predict a smaller emitting region observed at a shorter radio wavelength.





Supplementary Figure 1— **Measured (FWHM) angular size of Sgr A* vs. observing wavelength.** Blue and green lines represent the best-fit scattering relations of $1.39\lambda^2$ and $0.69\lambda^2$ along the major and minor axes, respectively. Black data points (open and filled circles) are size measurements from the quasi-simultaneous observations in February 1997 with the VLBA plus one antenna of the VLA. Red data points are from the best VLBI observations ever made, in terms of the recording rate (thus the sensitivity) and the weather condition, at 7 mm (open and filled diamond) and 3.5 mm (open and filled square), respectively. Here, open symbols are for major axis sizes and filled symbols are for minor axis sizes. 1σ error bars are plotted. See Supplementary Information and Table 1 for details.



Supplementary Information

Details of Model Fitting Procedure for the Source Structure Determination

An accurate determination of the apparent size of Sgr A* from the conventional VLBI imaging technique has suffered from calibration uncertainties. The southerly declination of Sgr A* ($\sim -30^\circ$) and northern latitudes for most of the existing VLBI antennas result in poor north-south resolution, which happens to be along the minor axis direction of the scattering structure. Furthermore, atmospheric effects, especially at shorter wavelengths, severely affect the amplitude calibration which is crucial to the determination of the structure of Sgr A*.

To minimize the calibration errors and thus to improve the accuracy of the apparent source structure measurements, we have developed a model fitting method by implicitly using the amplitude closure relation^{S1}. The major difference between this method and the widely used self-calibration technique for VLBI imaging lies in the way of obtaining the model of source brightness distribution. Both algorithms converge to consistent results with high signal-to-noise (SNR) data. The biggest drawback of the traditional imaging process is the non-uniqueness of the final image. This becomes more severe when weaker detections are involved, as in the case for the VLBI observations of Sgr A* where the λ^2 -dependent scattering image is always resolved out on the long to intermediate baselines, depending on the observing wavelength. The model fitting with the closure amplitude constraints is free from any antenna-dependent amplitude errors, and decides on the best fitted model by searching over all the possible models. This proved highly effective in dealing with the Sgr A* observations when the radio emission of Sgr A* can be represented by an elliptical Gaussian of 3 parameters, i.e. sizes of major axis (Θ_{major}) and minor axis (Θ_{minor}) and, the position angle (PA) of the major axis (East of North). This is because that the closure phases, as a direct measure of the asymmetry in source structure,

are measured to be consistent with a zero value. There are some data points deviating from the zero closure phases but having larger uncertainties. We thus restrict our model fitting to a single Gaussian component whose brightness distribution is symmetric with zero visibility phases. So, only the visibility amplitude is used in the model fitting. Before fitting, we performed a bias correction by solving two equations of the second and fourth moments of the measured visibility amplitude^{S1-S3}. The best-fit model of the source structure is obtained by minimizing χ^2 which is the weighted sum of the squared difference between the model and the measured (bias-corrected) visibility amplitudes over all the available baselines throughout the whole observation. In practice, a thorough search for minimum chi squares χ_{\min}^2 is carried out in the 3-dimensional space that covers a wide range of the three model parameters (Θ_{major} , Θ_{minor} and PA). This procedure is applicable to any source whose brightness distribution is characterized as a single Gaussian component.

For the error estimation, in case that χ_v^2 at χ_{\min}^2 is larger than unity, we scale up the 68.3% confidence region (corresponding to the formal standard error 1σ) as an increase of χ^2 from χ_{\min}^2 to $\chi_{\min}^2 + \Delta\chi^2$ with $\Delta\chi^2 = \chi_{\min}^2 / N_{\text{dof}}$. Here, N_{dof} is the summation of the difference between the number of visibilities N_{vis} and the number of antennas N_{ant} over all scans, minus the number of fitting parameters (3 for an elliptical Gaussian model), i.e. $N_{\text{dof}} = \sum_t (N_{\text{vis}} - N_{\text{ant}}) - 3$. By projecting this confidence contour onto the axis of parameter of interest, we can finally obtain 1σ for that single parameter.

Details of Revision of the Wavelength-dependent Scattering Law

The consistent departure of the fitted 7 mm apparent major axis size from the pure scattering size predicted by the current scattering model seen in all seven epochs (Table 1) seems to imply that the intrinsic source size of Sgr A* at 7 mm has already added significantly in quadrature to the scattering size in producing the observed deviation.

However, this conclusion explicitly assumes that the adopted wavelength-dependent scattering law is accurate enough. To check whether the difference is really due to intrinsic structure effect or an illusion caused by the inaccuracy of the current scattering model, we carry out weighted least-squares fit to the size measurements as a function of the observing wavelength. The weighting function is inversely proportional to the variance of the fitted size in Table 1. To minimize any temporal structural variability, all data points used except that at 3.5 mm are from near-simultaneous observations in February 1997 with the VLBA plus one antenna of the VLA.

Supplementary Figure 1 and Supplementary Table 1 summarize various trials. The power-law form $\Theta = \Theta^{\text{lcm}} \lambda^\alpha$ was adopted in the fitting. The different trials made use of various subsets of the data in order to test the impact of including the shortest wavelength (λ_{min}) as well as the longest wavelength (λ_{max}) data, and also allowing the power law index α to be a free parameter in the fitting or fixed to the value of 2 as predicted by the scattering theory. For the major axis, we first tried to fit four subsets with $\lambda_{\text{min}} = 0.348, 0.695, 1.350$ and 1.953 cm, respectively, and $\lambda_{\text{max}} = 6.02$ cm. The best-fit model of $\Theta_{\text{major}} = (1.51 \pm 0.06) \lambda^{1.88 \pm 0.05}$ (errors are 1σ) is obtained from the subset with $\lambda_{\text{min}} = 1.953$ cm. With a constant $\alpha = 2$, two subsets with $\lambda_{\text{min}} = 1.350$ and 1.953 cm, can be fit by the same $\Theta_{\text{major}} = (1.38 \pm 0.02) \lambda^2$. Thus, it is clear that the inclusion of 0.694 cm data did not lead to the best fitting in these fits for the major axis. The scattering size at 6.02 cm is heavily resolved by the VLBA. This severely limits the usable dataset. In particular, the fitted minor axis size could be arbitrarily small due to the poor constraint from the VLBA data along the North-South direction. As such, we tried the model fitting to a new sub-dataset with $\lambda_{\text{min}} = 1.953$ cm and $\lambda_{\text{max}} = 3.564$ cm. The fitting results are $\Theta_{\text{major}} = (1.39 \pm 0.05) \lambda^{2.00 \pm 0.06}$ (varying α) and $\Theta_{\text{major}} = (1.39 \pm 0.02) \lambda^2$ ($\alpha = 2$), respectively. Both fitting results are much better than above-mentioned fits. And, the fitted amplitudes Θ^{lcm} from both fits are identical and, the fitted exponential index

$\alpha = 2.00 \pm 0.06$ is indistinguishable from the fixed number of 2. We thus conclude from these tests that $\Theta_{\text{major}} = (1.39 \pm 0.02)\lambda^2$ is the best-fit scattering law along the major axis direction. By assuming that the λ^2 -dependence derived for the major axis also applies to the minor axis, we can obtain the best-fit wavelength-dependent minor axis size $\Theta_{\text{minor}} = (0.69 \pm 0.06)\lambda^2$ from fitting to the subset of data with $\lambda_{\text{min}} = 1.35$ cm. This newly revised wavelength-dependent two-dimensional scattering structure is also consistent with results from fitting to the closure amplitudes of somewhat different databases (STable 3 in ref. S4).

λ_{min} (cm)	λ_{max} (cm)	varying power law index α			fixed power law index α		
		$\Theta^{1\text{cm}}$ (mas)	α	χ_v^2	$\Theta^{1\text{cm}}$ (mas)	α	χ_v^2
0.348	6.020	1.45 ± 0.01	1.93 ± 0.02	1.27	1.42 ± 0.01	2	4.92
0.694	6.020	1.44 ± 0.01	1.94 ± 0.02	1.28	1.41 ± 0.01	2	5.22
1.350	6.020	1.46 ± 0.04	1.92 ± 0.04	1.83	1.38 ± 0.02	2	2.92
1.953	6.020	1.51 ± 0.06	1.88 ± 0.05	1.21	1.38 ± 0.02	2	4.37
1.953	3.564	1.39 ± 0.05	2.00 ± 0.06	0.11	1.39 ± 0.02	2	0.05

Supplementary Table 1. Summary of power-law fits to the major axial size of Sgr A* as a function of the observing wavelength.

S1. Shen, Z.-Q., Liang, M. C., Lo, K. Y. & Miyoshi, M. Searching for Structural Variability in Sgr A*. *Astron. Nachr.* **324**, S1, 383-389 (2003).

S2. Thompson, A. R., Moran, J. M. & Swenson, G. W. Interferometry and Synthesis in Radio Astronomy. New York: Wiley-Interscience. First (1991) and second (1994) reprintings by Krieger Pub. Co., Malabar (Florida) p260.

S3. Rogers, A. E. E., Doeleman, S. S. & Moran, J. M. Fringe Detection Methods for Very Long Baseline Arrays. *Astron. J.* **109**, 1391-1401 (1995).

S4. Bower, G. C. *et al.* Detection of the Intrinsic Size of Sagittarius A* Through Closure Amplitude Imaging. *Science* **304**, 704-708 (2004).

A size of ~ 1 AU for the radio source Sgr A* at the centre of the Milky Way

Zhi-Qiang Shen¹, K. Y. Lo², M.-C. Liang³, Paul T. P. Ho^{4,5} & J.-H. Zhao⁴

¹*Shanghai Astronomical Observatory, 80 Nandan Road, Shanghai 200030, China*

²*National Radio Astronomy Observatory, 520 Edgemont Road, Charlottesville, VA 22903, USA*

³*Division of Geological and Planetary Sciences, California Institute of Technology, Pasadena, CA 91125, USA*

⁴*Harvard-Smithsonian CfA, 60 Garden Street, Cambridge, MA 02138, USA*

⁵*Institute of Astronomy & Astrophysics, Academia Sinica, PO Box 23-141, Taipei 106, Taiwan, China*

Although it is widely accepted that most galaxies have supermassive black holes (SMBHs) at their centers¹⁻³, concrete proof has proved elusive. Sagittarius A* (Sgr A*)⁴, an extremely compact radio source at the center of our Galaxy, is the best candidate for proof⁵⁻⁷, because it is the closest. Previous Very Long Baseline Interferometry (VLBI) observations (at 7mm) have detected that Sgr A* is ~ 2 astronomical unit (AU) in size⁸, but this is still larger than the “shadow” (a remarkably dim inner region encircled by a bright ring) arising from general relativistic effects near the event horizon⁹. Moreover, the measured size is wavelength dependent¹⁰. Here we report a radio image of Sgr A* at a wavelength of 3.5mm, demonstrating that its size is ~ 1 AU. When combined with the lower limit on its mass¹¹, the lower limit on the mass density is $6.5 \times 10^{21} M_{\text{sun}} \text{pc}^{-3}$, which provides the most stringent evidence to date that Sgr A* is an SMBH. The power-law relationship between wavelength and intrinsic size (size \propto wavelength^{1.09}),

explicitly rules out explanations other than those emission models with stratified structure, which predict a smaller emitting region observed at a shorter radio wavelength.

Past VLBI observations¹²⁻¹⁶ of Sgr A* have revealed an east-west elongated structure whose apparent angular size at longer wavelengths is dominated by the interstellar scattering angle, i.e. $\Theta_{\text{obs}} = \Theta_{\text{obs}}^{\text{1cm}} \lambda^2$, where λ is the wavelength in cm, and Θ_{obs} is the observed size in milli-arc second (mas). Thus, VLBI observations at shorter millimetre wavelengths where the intrinsic structure of Sgr A* could become comparable to the pure scattering size, are expected to show deviations of the observed size from the scattering law. This has been demonstrated by the recent detection of the intrinsic size at 7 mm (ref. 8). On November 3, 2002, we successfully carried out an observation of Sgr A* with the Very Long Baseline Array (VLBA) at its shortest wavelength of 3.5 mm (ref. 10). Our observation, with the steadily improved performance of the VLBA system, has produced the first high-resolution image of Sgr A* ever made at 3.5 mm (Fig. 1), which exhibits an elongated structure too.

To yield a quantitative description of the observed structure, we tried a model fitting procedure¹⁷ in which the amplitude closure relation is applied. Compared to the conventional VLBI self-calibration and imaging technique, this can improve on the calibration of current VLBI observations of Sgr A* (see Supplementary Information). We have applied this model fitting procedure to twelve sets of VLBA observations of Sgr A* made at a variety of wavelengths from 6 cm to 3.5 mm over the time range from 1994 to 2004. Two experiments at 7 mm in 1994 are from VLBA archive. Table 1 lists the fitting results. A consistent position angle ($\sim 80^\circ$) of the scatter-broadened image can be seen in all the datasets, regardless of the observing epoch and wavelength. Furthermore, it is quite significant that in all seven experiments made at 7 mm, the fitted apparent major axis size is always larger than the largest known scattering size of 0.69

mas extrapolated from the existing scattering models. We thus perform weighted least-squares fit to the near-simultaneous angular size measurements (in February 1997) as a function of the observing wavelength (see Supplementary Information for more details). We conclude that the best-fit two-dimensional scattering structure is $\Theta_{\text{major}} = (1.39 \pm 0.02)\lambda^2$ by $\Theta_{\text{minor}} = (0.69 \pm 0.06)\lambda^2$ with a position angle of $\sim 80^\circ$. This gives an even smaller scattering angle along the major axis direction. An immediate important conclusion is that the discrepancy seen in all 7-epoch 7 mm VLBI observations is real, implying the appearance of the intrinsic source structure at wavelengths of 7 mm and shorter (see Supplementary Figure 1).

At 7 mm, two measurements from the March 2004 observations are used to get averaged sizes of the major and minor axes of 0.724 ± 0.001 and 0.384 ± 0.013 mas, respectively with position angle $80.6_{-0.6}^{+0.5}$ degrees. The difference between the measured and the extrapolated scattering sizes along the major axis is $\Delta\Theta = 0.053 \pm 0.010$ mas, significant at $> 5\sigma$ level. By subtracting in quadrature the scattering angle, this suggests an intrinsic size of 0.268 ± 0.025 mas for the major axis. Similarly, we can derive an intrinsic size for the minor axis to be 0.190 ± 0.057 mas, comparable to the major axis size. However, it should be kept in mind that the deviation seen for the minor axis is only significant at 1.6σ level. Note that the derived source size has greater statistical significance than the deviation, because the scattering size has been deduced with good accuracy.

At 3.5 mm, the fitted apparent source structure from November 2002 VLBA observations is $0.21_{-0.01}^{+0.02}$ mas by $0.13_{-0.13}^{+0.05}$ mas with a position angle of 79_{-33}^{+12} (see Table 1). Thus, for the first time an intrinsic size of 0.126 ± 0.017 mas for the major axis can be obtained from the deviation $\Delta\Theta = 0.042 \pm 0.010$ mas (at $> 4\sigma$ level) in the measured major axis size from that of scattering angle at 3.5 mm. Mainly due to the limited resolution, the minor axis measurement at 3.5 mm, however, is inadequate to

make any firm claim on the determination of its intrinsic size. So, we defer any estimate of intrinsic minor axis size at 3.5 mm for future investigation. Past 3.5 mm VLBI observations with the heterogeneous Coordinated Millimeter VLBI Array, severely limited by its low sensitivity, could not warrant a model more complex than the circular one¹⁸. The best-fit circular Gaussian has a diameter of 0.18 ± 0.02 mas, which is indistinguishable from the scattering size along the major axis and cannot give a meaningful estimate of the intrinsic structure⁸.

Thus we have sampled a zone of the SMBH closer to the event horizon than ever before, by detecting the intrinsic size of Sgr A* to be only 1.01 AU at a distance of 8.0 kpc, or $12.6R_{\text{sc}}$, where $R_{\text{sc}} (\equiv 1.2 \times 10^{12} \text{ cm})$ is the Schwarzschild radius of a $4 \times 10^6 M_{\text{sun}}$ SMBH. By assuming a spherical structure, we obtain a lower limit to the mass density of Sgr A* of $6.5 \times 10^{21} M_{\text{sun}} \text{ pc}^{-3}$. Here, we used the lower bound to the mass of Sgr A*, derived from the upper limit to the intrinsic proper motion of Sgr A* itself¹¹, which is about 10% of the $4 \times 10^6 M_{\text{sun}}$ inferred from the stellar orbital motions⁶⁻⁷, and the upper limit to the source intrinsic size (this work). This mass density is at least 4 orders of magnitude greater than that determined from dynamical measurements of stellar velocities⁶. This is because here we are probing directly the structure of Sgr A*, where the assumed mass estimate refers to the value within Sgr A*. We note also that this mass density is almost 12 orders of magnitude greater than the estimate for NGC 4258 (ref. 19), one of the best known SMBHs. Such an extraordinarily high mass density robustly rules out the possibility of Sgr A* being a compact dark cluster of stellar remnants as it would have an unreasonably short lifetime of less than 100 yrs (ref. 20), and thus argues strongly in favor of the SMBH nature of Sgr A*. To prove that Sgr A* is indeed an SMBH requires an unambiguous demonstration that Sgr A* possesses an event horizon. It is intriguing that the detected intrinsic size at 3.5 mm is about two times the diameter of the shadow caused by the strong gravitational bending of light rays⁹. Thus, it is very promising that VLBI observations of Sgr A* at 1 mm or shorter

will reach the region comparable to its shadow, which can be used to differentiate between the SMBH scenario and other supermassive non-baryonic stars^{9, 21}.

The two-point fit to the well determined intrinsic sizes at 7 and 3.5 mm shows a λ^β -dependence of the intrinsic source size with $\beta = 1.09^{+0.34}_{-0.32}$ (Fig. 2). Also plotted in Fig. 2 are two inferred lower limits of 0.02 and 0.008 mas to the intrinsic size at 1.3 and 0.8 mm, respectively, from the absence of refractive scintillation²². These lower limits are consistent with the extrapolation of the λ^β -dependence. However, we note that these two lower limits are only about 2 and 0.8 R_{sc} , which are smaller than the last stable orbit (LSO) radius of 3 R_{sc} for a non-rotating (Schwarzschild) black hole. There is some evidence that Sgr A* is a rotating black hole²³. For a prograde maximally rotating Kerr black hole the LSO radius is 0.5 R_{sc} . The LSO establishes the lower limit to the emission region size. Hence the λ^β -dependence will eventually reach a minimum. As such, the turn-over frequency²⁴ seen in the entire spectrum of Sgr A* might tell us the smallest size of the emission, which can be further used to constrain its spin, if any.

The extrapolated intrinsic size at 1.35 cm is $0.555^{+0.136}_{-0.115}$ mas. This, when compared to the scattering angle of 2.576 ± 0.036 mas, is consistent with the idea that the scattering effect dominates the observed source size at 1.35 cm. This deduced source size is also formally consistent with the reported detection of $0.726^{+0.152}_{-0.111}$ mas, to within the uncertainties⁸.

The derived $\lambda^{1.09}$ -dependence requires that the emission at different wavelengths is dominated by different emitting region and thus conclusively exclude those models without the stratified emission structure. Along with the detected intrinsic major axis size, we can derive a lower limit to the intrinsic brightness temperature as $T_{\text{b}} \geq 1.36 \times 10^9 \times \frac{S_\lambda \lambda^2}{\Theta_{\text{int}}^2}$ K; here S_λ is the flux density in Jy at wavelength λ in cm and Θ_{int} is the intrinsic major axis size in mas. There is a wavelength dependence of the

lower limit T_b as $\lambda^{-\alpha-0.18}$ (assuming $S_\lambda \propto \lambda^{-\alpha}$). Using the flux densities of 1.0 and 1.2 Jy at 7 and 3.5 mm, respectively, the corresponding minimal T_b is 0.9×10^{10} and 1.2×10^{10} K, greater than the prediction of the spherical accretion model²⁵. However, this lower limit of 10^{10} K, and the spatial distribution of the radio emission, can be explained easily by the inhomogeneous jet model²⁶⁻²⁷, in which the magnetic field and the electron number density vary with the distance (r) to the origin of the jet as r^{-1} and r^{-2} , respectively. On the other hand, the radiatively inefficient accretion flow (RIAF) model of Sgr A* (ref. 28) can also account for a brightness temperature of $>10^{10}$ K as well as the observed spectral energy distribution. The prediction of $\lambda^{0.9}$ from the hybrid thermal-nonthermal synchrotron radiation from RIAF (ref. 29) is in agreement with the estimated $\lambda^{1.09^{+0.34}_{-0.32}}$ relation. Here, the possible existence of strong outflows from the accretion disk was not taken into account. To further discern between them, it is important to study the correlation between the detected X-ray variability and the variations frequently seen in the radio to sub-millimetre wavelengths, which would yield further information on the intrinsic density structure of the emitting zone.

<received> Style tag for received and accepted dates (omit if these are unknown).

1. Begelman, M. C. Evidence for Black Holes. *Science* **300**, 1898-1903 (2003).
2. Kormendy, J. & Richstone, D. Inward Bound – The Search for Supermassive Black Holes in Galactic Nuclei. *Annu. Rev. Astron. Astrophys.* **33**, 581-624 (1995).
3. Rees, M. J. Black Hole Models for Active Galactic Nuclei. *Annu. Rev. Astron. Astrophys.* **22**, 471-506 (1984).
4. Balick, B. & Brown, R. L. Intense sub-arcsecond structure in the Galactic Center. *Astrophys. J.* **194**, 265-270 (1974).
5. Melia, F. & Falcke, H. The supermassive black hole at the Galactic Center. *Annu. Rev. Astron. Astrophys.* **39**, 309-352 (2001).

6. Schödel, R. *et al.* A star in a 15.2 year orbit around the supermassive black hole at the centre of the Milky Way. *Nature* **419**, 694-696 (2002).
7. Ghez, A. M. *et al.* Stellar orbits around the Galactic Center black hole. *Astrophys. J.* **620**, 744-757 (2005).
8. Bower, G. C. *et al.* Detection of the Intrinsic Size of Sagittarius A* Through Closure Amplitude Imaging. *Science* **304**, 704-708 (2004).
9. Falcke, H., Melia, F. & Agol, E. Viewing the shadow of the black hole at the Galactic Center. *Astrophys. J.* **528**, L13-L16 (2000).
10. Shen, Z.-Q. & Lo, K. Y. High-resolution 86 GHz VLBA imaging of Sgr A*. *Progress of Theoretical Physics Supplement* **155**, 413-414 (2004).
- 11 Reid, M. *et al.* The position, motion, and mass of Sgr A*. *Astron. Nachr.* **324**, S1, 505-511 (2003).
12. Davies, R. D., Walsh, D. & Booth, R. S. The radio source at the Galactic nucleus. *Mon. Not. R. Soc.* **177**, 319-333 (1976).
13. Lo, K. Y. *et al.* On the size of the galactic centre compact radio source diameter less than 20 AU. *Nature* **315**, 124-126 (1985).
14. Alberdi, A. *et al.* VLBA Image of Sagittarius-A* at Lambda = 1.35-Centimeters. *Astron. Astrophys.* **277**, L1- L4 (1993).
15. Bower, G. C. & Backer, D. C. 7 Millimeter VLBA Observations of Sagittarius A*. *Astrophys. J.* **496**, L97-100 (1998).
16. Lo, K. Y., Shen, Z.-Q., Zhao, J.-H. & Ho, P. T. P. Intrinsic Size of Sagittarius A*: 72 Schwarzschild Radii. *Astrophys. J.* **508**, L61-64 (1998).
17. Shen, Z.-Q., Liang, M. C., Lo, K. Y. & Miyoshi, M. Searching for Structural Variability in Sgr A*. *Astron. Nachr.* **324**, S1, 383-389 (2003).

18. Doeleman, S. S. *et al.* Structure of Sagittarius A* at 86 GHz using VLBI Closure Quantities. *Astron. J.* **121**, 2610-2617 (2001).
19. Miyoshi, M. *et al.* Evidence for a Black-Hole from High Rotation Velocities in a Sub-Parsec Region of NGC4258. *Nature* **373**, 127-129 (1995).
20. Maoz, E. Dynamical Constraints on Alternatives to Supermassive Black Holes in Galactic Nuclei. *Astrophys. J.* **494**, L181-L184 (1998).
21. Torres, D. F., Capozziello, S. & Lambiase, G. Supermassive boson star at the galactic center? *Phys. Rev. D.* **62**, 104012 (2000).
22. Gwinn, C. R., Danen, R. M., Tran, T. Kh., Middleditch, J. & Ozernoy, L. M. The Galactic center radio source shines below the Compton limit. *Astrophys. J.* **381**, L43-L46 (1991).
23. Genzel, R. *et al.* Near-infrared flares from accreting gas around the supermassive black hole at the Galactic Centre. *Nature* **425**, 934-937 (2003).
24. Falcke, H. *et al.* The simultaneous spectrum of Sagittarius A* from 20 centimeter to 1 millimeter and the nature of the millimeter excess. *Astrophys. J.* **499**, 731-734 (1998).
25. Melia, F. An accretion black hole model for Sagittarius A*. II. A detailed study. *Astrophys. J.* **426**, 577-585 (1994).
26. Königl, A. Relativistic Jets as X-ray and Gamma-ray Sources. *Astrophys. J.* **243**, 700-709 (1981).
27. Falcke, H. & Markoff, S. The jet model for Sgr A*: Radio and X-ray spectrum. *Astron. Astrophys.* **362**, 113- 118 (2000).
28. Yuan, F., Quataert, E. & Narayan, R. Nonthermal Electrons in Radiatively Inefficient Accretion Flow Models of Sagittarius A*. *Astrophys. J.* **598**, 301-312 (2003).
29. Özel, F., Psaltis, D. & Narayan, R. Hybrid Thermal-Nonthermal Synchrotron Emission From Hot Accretion Flows. *Astrophys. J.* **541**, 234-249 (2000).

Supplementary Information is linked to the online version of the paper at www.nature.com/nature.

Acknowledgements The Very Large Array and the Very Long Baseline Array are operated by the National Radio Astronomy Observatory, which is a facility of the National Science Foundation, operated under cooperative agreement by Associated Universities Inc. Z.-Q. Shen acknowledges the support by the One-Hundred-Talent Program of Chinese Academy of Sciences.

Author Information Reprints and permissions information is available at npg.nature.com/reprintsandpermissions. The authors declare no competing financial interests. Correspondence and requests for materials should be addressed to Z.-Q.S. (zshen@shao.ac.cn).

Figure 1: The first high-resolution VLBI image of Sgr A* at 3.5 mm obtained with the VLBA on November 3, 2002. The observations were dynamic scheduled to ensure the good weather conditions at most sites, and the data were recorded at the highest possible recording rate of 512 Mbps (Mega Bits Per Second). Standard visibility amplitude calibration including the elevation-dependent opacity correction was done, and the final image was obtained after several iterations of the self-calibration and cleaning procedures. The calibrated total flux density is about 1.2 Jy. **a**, A uniformly weighted image with the restoring beam (indicated at the lower left corner) of $1.13 \text{ mas} \times 0.32 \text{ mas}$ at 9° . The peak flux density is $1.08 \text{ Jy beam}^{-1}$. Contour levels are drawn at $3\sigma \times (-1, 1, 2, 4, 8, 16, 32)$, $3\sigma = 17.5 \text{ mJy beam}^{-1}$. **b**, A super-resolution image with a circular beam of 0.20 mas from which an east-west elongated structure can be seen (see Table 1). Note the different scales. The contour levels are the same as that in **a** with the corresponding peak flux density of $1.01 \text{ Jy beam}^{-1}$.

Figure 2: Intrinsic major axis size vs. observing wavelength. The solid line represents the two-point fit from the detected intrinsic sizes at both 3.5 and 7 mm (this work). Also plotted are the lower limits to the intrinsic sizes at 1.3 and 0.8 mm (ref. 22), and the reported detection at 1.35 cm (ref. 8). The extrapolated intrinsic sizes at 1.3 and 0.8 mm

are about $4.3R_{\text{sc}}$ and $2.5R_{\text{sc}}$, respectively. Here, R_{sc} ($\equiv 1.2 \times 10^{12}$ cm) is the Schwarzschild radius for a $4 \times 10^6 M_{\text{sun}}$ SMBH.

Table 1. Parameters of the elliptical Gaussian model for Sgr A*

λ	ν (bw, rate) ^a	Epoch	Θ_{major} ^{b,d}	Θ_{minor} ^{b,d}	PA ^d
(cm)	(GHz) (MHz, bits)	(d m y)	(mas)	(mas)	($^{\circ}$)
0.348	86.236 (128,2)	03Nov2002	$0.21^{+0.02}_{-0.01}$	$0.13^{+0.05}_{-0.13}$	79^{+12}_{-33}
0.694	43.213 (32,2) ^c	14Feb1997	$0.71^{+0.01}_{-0.01}$	$0.42^{+0.05}_{-0.05}$	74^{+2}_{-2}
0.695	43.175 (128,2)	08Mar2004	$0.722^{+0.002}_{-0.002}$	$0.395^{+0.019}_{-0.020}$	$80.4^{+0.8}_{-0.8}$
0.695	43.175 (128,2)	20Mar2004	$0.725^{+0.002}_{-0.002}$	$0.372^{+0.020}_{-0.018}$	$80.8^{+0.6}_{-0.9}$
0.695	43.151 (64,1)	26Apr1994	$0.72^{+0.01}_{-0.01}$	$0.39^{+0.07}_{-0.07}$	78^{+2}_{-2}
0.695	43.151 (64,1)	29Sep1994	$0.72^{+0.01}_{-0.01}$	$0.42^{+0.03}_{-0.03}$	79^{+1}_{-1}
0.695	43.135 (32,2)	24Apr1999	$0.69^{+0.01}_{-0.01}$	$0.33^{+0.04}_{-0.04}$	83^{+1}_{-1}
0.695	43.135 (32,2)	23May1999	$0.71^{+0.01}_{-0.01}$	$0.44^{+0.02}_{-0.02}$	79^{+1}_{-1}
1.350	22.229 (32,1) ^c	12Feb1997	$2.53^{+0.06}_{-0.05}$	$1.45^{+0.23}_{-0.38}$	83^{+4}_{-5}
1.953	15.361 (32,1) ^c	12Feb1997	$5.33^{+0.07}_{-0.07}$	$2.70^{+0.30}_{-0.44}$	83^{+3}_{-3}
3.564	8.417 (32,1) ^c	07Feb1997	$17.5^{+0.5}_{-1.0}$	$8.5^{+1.0}_{-1.0}$	87^{+3}_{-3}
6.020	4.983 (32,1) ^c	07Feb1997	$43.0^{+2.5}_{-1.0}$		

Results from the model fitting procedure which implicitly uses the amplitude closure relation (see Supplementary Information for details). Also listed are some details of the VLBI observations. Except five observations in February 1997 which used the VLBA and one VLA antenna, all the other observations were performed by the VLBA.

^a the observing frequency in GHz. Numbers in parenthesis are the recording bandwidth in MHz and the sampling rate (1 bit or 2 bits). With the same total bandwidth, the noise level from 2-bit quantization data is about $\sqrt{2}$ times lower than that from 1-bit quantization. The recording rate is two times the product of the bandwidth and the sampling rate.

^b full width half maximum (FMHM)

^c dual polarization observation. Both left and right circular polarization data have the same recording mode (listed) and, both data were used in the model fitting.

^d in all cases, errors are 1σ